Coassembled Cytotoxic and Pegylated Peptide Amphiphiles Form Filamentous Nanostructures with Potent Antitumor Activity in Models of Breast Cancer

Daniel J. Toft,[†,‡] Tyson J. Moyer,[†,§] Stephany M. Standley,[†,§] Yves Ruff,[†,⊥] Andrey Ugolkov,[‡] Samuel I. Stupp,[†,‡,§,⊥,*] and Vincent L. Cryns[†,‡,∥,*]

[†]Institute for BioNanotechnology in Medicine, Northwestern University, Chicago, Illinois 60611, United States, [‡]Department of Medicine, Robert H. Lurie Comprehensive Cancer Center, Feinberg School of Medicine, Northwestern University, Chicago, Illinois 60611, United States, [§]Department of Materials Science & Engineering, Northwestern University, Evanston, Illinois 60208, United States, and [⊥]Department of Chemistry, Northwestern University, Evanston, Illinois 60208, United States. [∥]Present address: Department of Medicine, Carbone Cancer Center, University of Wisconsin School of Medicine and Public Health, Madison, Wisconsin 53705, United States. D. J. Toft and T. J. Moyer contributed equally to this work. S. I. Stupp and V. L. Cryns contributed equally to this work.

ABSTRACT Self-assembled peptide amphiphiles (PAs) consisting of hydrophobic, hydvrogen-bonding, and charged hydrophilic domains form cylindrical nanofibers in physiological conditions and allow for the presentation of a high density of bioactive epitopes on the nanofiber surface. We report here on the use of PAs to form multifunctional nanostructures with tumoricidal activity. The combination of a cationic, membrane-lytic PA coassembled with a serum-protective, pegylated PA was shown to self-assemble into nanofibers. Addition of the pegylated PA to the nanostructure substantially limited degradation of the cytolytic PA by the protease trypsin, with an 8-fold increase in the amount of intact PA observed after digestion. At the same time, addition of up to 50% pegylated PA to the nanofibers did not decrease the *in vitro* cytotoxicity of the cytolytic PA. Using a fluorescent tag covalently attached to PA nanofibers we were able to track the biodistribution in plasma and tissues of tumor-bearing mice over time after intraperitoneal administration of the nanoscale filaments. Using an orthotopic mouse xenograft model of breast cancer, systemic administration of the cytotoxic pegylated nanostructures significantly reduced tumor cell proliferation and overall tumor growth, demonstrating the potential of multifunctional PA nanostructures as versatile cancer therapeutics.

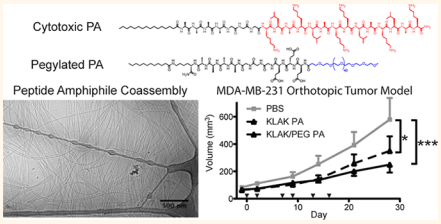

KEYWORDS: peptide amphiphile · cancer therapy · nanofiber · breast cancer · pegylation

Nanotechnology offers great potential to improve conventional cancer therapies through enhancement of both drug delivery and antitumor activity.[1,2] Nanoparticles in the size range of tens to hundreds of nanometers can passively accumulate in tumors due to their leaky vasculature and poor lymphatic clearance, referred to as the enhanced permeability and retention (EPR) effect.[3] In addition to size, the shape of the nanostructures plays an important role in tumor and cell uptake. Examples of nonspherical cell-penetrating particles existing in nature include the filamentous viruses such as the tobacco mosaic virus and the potato virus X.[4] Inspired by these examples from biology, Discher *et al.* have shown that cylindrical micelles have longer circulation times relative to spherical controls.[5] Maximum tolerated doses also increase with cylinders compared to spherical block copolymers.[6] Furthermore, particles with higher aspect ratios have shown increased uptake into cancer cells.[7]

Lipidated peptides with certain sequences were identified by our group as a broad class of small molecules that self-assemble into cylindrical nanostructures.[8,9] This family of peptide amphiphiles (PAs) are synthesized using solid-phase peptide synthesis by attaching an alkyl tail to a short peptide sequence that is typically composed of a β-sheet-forming region that drives cylinder formation and a bioactive signaling epitope, which may include charged residues to promote water solubility. PAs spontaneously self-assemble in aqueous solution into high-aspect-ratio filaments through hydrophobic collapse of alkyl segments to form the core of the nanofiber and by hydrogen bonding among peptide segments to create β-sheet structures. The resultant nanostructures can be designed to display bioactive peptide epitopes at high density on their surfaces.[10] PAs have been investigated *in vivo* as therapies in regenerative medicine, including central nervous system repair, bone and cartilage regeneration,

* Address correspondence to s-stupp@northwestern.edu, vlcryns@medicine.wisc.edu.

Received for review June 6, 2012 and accepted August 10, 2012.

Published online August 28, 2012
10.1021/nn302503s

angiogenesis for hind limb ischemia, and myocardial infarction.[11−16] In addition, our group has shown previously that treating mice bearing orthotopic human breast tumors with soluble PA nanostructures encapsulating hydrophobic chemotherapy in the core of the fibers has reduced tumor burden.[17]

The tunable nature of peptide-based therapeutics allows for the precise targeting of extracellular or intracellular components to induce cancer cell death.[18,19] Additional potential advantages of therapeutic peptides include complete biodegradability into benign metabolites and ease of synthesis. Peptides have shown promise as potential cancer therapeutics in a variety of models. For example, the α-helical cationic peptide sequence $(KLAKLAK)_2$ was shown to interact strongly with lipid membranes.[20] This peptide, commonly conjugated to cell-penetrating or -targeting peptides, lyses either plasma or mitochondrial membranes and has shown antitumor activity *in vivo*.[21−23]

Our group has previously described a PA that contains the membrane-lytic, highly cationic $(KLAKLAK)_2$ sequence as the bioactive component.[24] This PA (referred to here as KLAK PA) has the sequence $C_{16}A_4G_3(KLAKLAK)_2$ and assembles into cylindrical nanostructures capable of disrupting cell membranes.[24] An interesting characteristic of KLAK PA is that the delivery vector is also the therapy, whereas most other nanoscale delivery vehicles encapsulate traditional chemotherapies or have incorporated biologic therapies into nonbiodegradable nanoparticles.[25] We previously showed that KLAK PA nanostructures were more cytotoxic toward transformed cells compared with untransformed cells.[24] We speculate that this effect is due to the increased amount of negative charge on the surface of cancer cells.[26] KLAK PA nanoparticles may be passively targeted to tumors *in vivo* through the EPR effect, but it is possible that the KLAK epitope mediates active targeting: The R/KXXR/K epitope has shown potential for tumor targeting, which suggests that the membrane-lytic KLAK sequence could also function to increase tumor uptake.[27]

Because peptides can be quickly degraded after systemic delivery, ongoing work has investigated limiting proteolysis in circulation.[28,29] A common strategy is to synthesize peptides using D-enantiomers that are more resistant to endogenous protease degradation.[29,30] Another strategy to improve the therapeutic-delivery vehicle is to functionalize the surface with polymers that protect from proteolysis, lessen immune response, and improve circulation time. Polyethylene glycol (PEG) is widely known to reduce the metabolism and elimination of pegylated molecules in the bloodstream.[31] For instance, the covalent attachment of pegylated-lipid micelles to short peptide sequences has been shown to decrease the rate of peptide

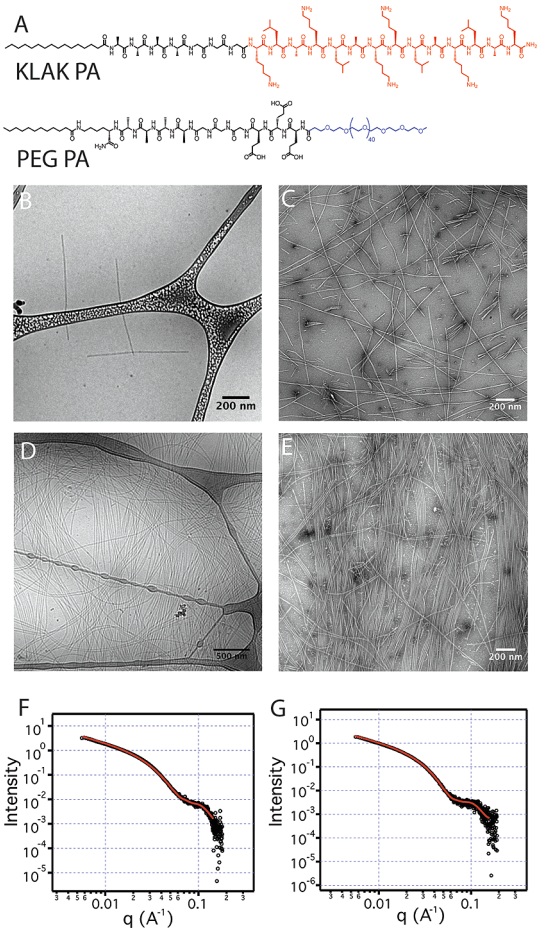

Figure 1. PA characterization. (A) Chemical structure of "KLAK PA" with the sequence palmitoyl-$A_4G_3(KLAKLAK)_2$ and "PEG PA" with the sequence PEG_{2000}-$E_3G_3A_4K(C_{12})$. Cryo-TEM of KLAK PA alone (B). KLAK with PEG (D) shows a significant difference in average length. Conventional TEM images show fiber formation for both KLAK alone (C) and KLAK PA with PEG PA (E). SAXS confirms the presence of cylindrical structures in solution for both KLAK mixed with PEG PA (F) and PEG PA alone (G).

proteolysis.[32] Doxil, a pegylated liposome that contains doxorubicin, enhances the circulation time compared to free doxorubicin and has a blood half-life of more than 48 h.[33] Variations in the molecular weight of PEG on polymersomes[34] and density of PEG on polymeric micelles[35] have been shown to induce drastic changes in circulation time and biodistribution. Furthermore, pegylation of the protein interferon has improved circulation time and efficacy against hepatitis C.[36] Pegylation of self-assembling peptides has been described previously,[37,38] and Hamley and co-workers have attached a PEG chain to a β-sheet-forming peptide that formed long, one-dimensional fibers.[39] However, the *in vivo* impact of pegylation on self-assembled peptide bioactivity has not yet been reported. Here we demonstrate the use of a coassembled combination of pegylated PA (PEG PA) and the cytotoxic KLAK PA to create an effective antitumor therapy.

RESULTS AND DISCUSSION

TEM and SAXS Characterization. The chemical structures of KLAK PA and PEG PA are shown in Figure 1A. Conventional and cryogenic transmission electron microscopy (TEM) were performed on the KLAK PA alone, PEG PA alone, and the KLAK/PEG PA mixture. KLAK PA appears to form short, cylindrical fibers that are roughly 10 nm in diameter and several hundred nanometers in length according to cryo-TEM (Figure 1B). Conventional TEM shows the presence of both short, bundled fibers and longer single fibers (Figure 1C). Overall, according to both the cryo and conventional TEM, KLAK PA forms relatively short fibers. PEG PA, on the other hand, forms fibers that are similar in diameter, but significantly longer in length (see Supporting Information for details, specifically Supplemental Figure S1). Three glutamic acids were included in the PEG PA structure to utilize electrostatic attraction during coassembly.[40] The two PAs were mixed in a 1:1 molar ratio to produce a coassembled structure. The PEG and KLAK PAs were first dissolved and mixed in hexafluoroisopropanol (HFIP), lyophilized, and resuspended in PBS. HFIP, known to disrupt hydrogen bonding, was used to destabilize the assembled structures and enhance coassembly of the two PAs. Cryo-TEM of the mixture shows that the longer fibers are the dominant morphology (Figure 1D), and the short, bundled structures that were observed in conventional TEM of KLAK PA alone were no longer visible in the coassembled structure (Figure 1E). The mixed KLAK–PEG PAs form longer structures with a similar morphology compared to the PEG alone. KLAK PA synthesized using D-enantiomers ("D-KLAK") showed similar morphologies both with and without PEG PA by conventional TEM, suggesting that the assembled structures were independent of the chirality of KLAK PA (Supplemental Figure S2). In both cases, short nanofibers were observed for KLAK PA alone, while the mixing of PEG PA and KLAK PA appeared to drastically increase the nanofiber length. We speculate that the difference in observed nanofiber lengths is due to the coassembly of oppositely charged molecules, which decreases the electrostatic barrier to the formation of long cylindrical structures.

Small-angle X-ray scattering (SAXS), a technique that can be used to determine the size and shape of nanostructures in solution, confirmed the presence of cylindrical structures in solution. We sought to verify that there was no visible change in supramolecular structure when KLAK PA and PEG PA molecules were mixed compared to solutions prepared only with PEG PA. Both the KLAK-PEG PA mixture and PEG PA alone had a slope of −1 in the low-q range, which is indicative of cylinders in solution. In the cases of KLAK PA without PEG PA, both KLAK and D-KLAK PA had slopes of approximately −2 in the low q-range, which could be

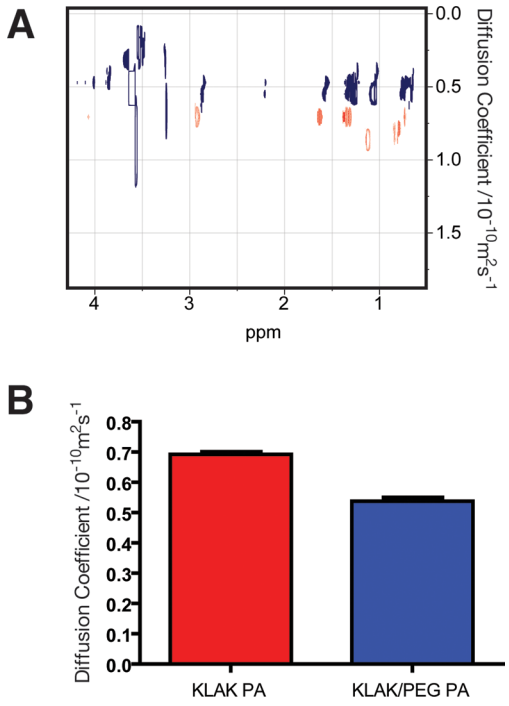

Figure 2. DOSY of coassembled structures. (A) Overlaid DOSY results for KLAK PA alone (red) and KLAK with PEG PA show a shift in the diffusion coefficient. (B) Using the KLAK PA peak at 2.83 ppm, the KLAK PA alone diffusion coefficient shows an increase upon mixing with PEG PA.

the result of bundling of multiple nanostructures together (Supplemental Figure S3). However, in order to accurately quantify the size of these nanostructures, core–shell cylinder models were used for each of the PAs. The KLAK–PEG PA mixture was fit to a polydisperse core–shell cylinder model (Figure 1F). The total radius, which includes core and shell thickness, was found to be 4.9 nm according to the fit, which is similar to the 4.3 nm fit radius of PEG PA alone (Figure 1G). We suggest that since the PEG chain is well hydrated, its electron density is indistinguishable from the solvent, causing the radius to appear smaller than expected. Thus, combining the results from TEM and SAXS, two possibilities exist: either KLAK PA is incorporated into the same nanostructure as PEG PA without significant disruption of fiber morphology or the PEG PA nanostructure is dominating the scattering and microscopy images. The observed increase in nanostructure radius from 4.3 to 4.9 nm upon addition of the KLAK PA lends support to the possibility that coassembly of both molecules indeed occurs in the observed supramolecular filaments.

DOSY. Diffusion-ordered spectroscopy (DOSY) measures the exponential attenuation of NMR signals while applying a pulsed-field gradient to determine the diffusion coefficient of each chemical species.[41] It has been used to distinguish a variety of nanostructures based on diffusion coefficients, including carbon nanotubes.[42] To assess changes in fiber diffusion

constants, we performed DOSY NMR on both KLAK PA alone and the mixture of KLAK and PEG PAs. Because individual spectral peaks can be monitored by DOSY, one can observe changes in diffusion of a specific molecule in a mixture of two or more components. DOSY results show a shift in the diffusion coefficient of the KLAK PA after addition of PEG PA (Figure 2A). All of the peaks in the blended sample with KLAK and PEG PAs correspond to the same diffusion coefficient, suggesting that both PAs are on the same nanostructure. A slight upfield shift in the KLAK PA alone peak at 1.2 ppm may be the result of more flexible peptides at the periphery of the nanostructure. One possible explanation for this effect is that the α-helical nature of the KLAK sequence decreases the interaction with surrounding molecules, thus increasing the translational diffusion coefficient. Additionally, comparing the diffusion coefficients by DOSY for KLAK PA with and without PEG PA showed a change in size after the addition of PEG PA, suggesting an interaction between the two molecules. To quantify this difference, we used the attenuation of the amplitude of an NMR signal from KLAK PA, which decays exponentially at a rate that is proportional to the diffusion coefficient. The peak at 2.83 ppm, which was attributed to KLAK PA using the 1H 1-D spectra (Supplemental Figures S4 and S5), was fitted to an exponential decay (Figure S6) and showed the same change in diffusion coefficient (Figure 2B). The KLAK PA alone diffusion coefficient was found to be 0.69×10^{-10} m^2/s, whereas when PEG PA molecules were mixed with KLAK PA, the diffusion coefficient was lowered to 0.54×10^{-10} m^2/s. We attribute this shift in diffusion coefficient to the incorporation of KLAK PA into a coassembled nanostructure with PEG PA, which corresponded with the change in size and morphology as determined by TEM and SAXS. These data collectively are indicative of coassembly of the two PA molecules in the same nanostructure.

Enzymatic Degradation. The addition of PEG PA to the KLAK PA fibers was intended to create a protective corona around the assembled nanostructure, which would limit nonspecific adsorption of proteins and reduce proteolysis. Protection from proteolysis is an important characteristic for effective peptide nanostructures in serum. To test the effect of including PEG PA on enzymatic degradation, we exposed the coassembled structure of KLAK PA and PEG PA to trypsin for one hour. Using this assay, we also determined an optimal amount of PEG PA to be coassembled with KLAK PA. Trypsin, which cleaves peptides on the C-terminal side of positively charged residues, was added to solutions of 250 μM KLAK PA, which contained varying concentrations of coassembled PEG PA. Because PEG PA has no cationic amino acids, trypsin will cleave peptides only on KLAK PA. After removal of trypsin, concentrations of intact KLAK PA were measured by liquid chromatography−mass spectroscopy (LC-MS). Significantly decreased levels of degradation of KLAK PA were observed for solutions that contained at least 50 mol % PEG PA relative to 25 mol % PEG PA and 0 mol % PEG PA (Figure 3). As an additional control, KLAK PA and PEG PA were preassembled in separate solutions prior to mixing and the addition of trypsin. In this case, the presence of 50% (molar) PEG PA had no effect on degradation of KLAK PA, and there was no statistically significant difference relative to the 0 mol % PEG PA control. These degradation results strongly suggest that KLAK PA and PEG PA are coassembled in the same nanostructure. For further biological testing, 50 mol % of PEG PA (a 1:1 molar ratio of KLAK PA to PEG PA) was used because additional PEG PA did not significantly reduce proteolysis of KLAK PA.

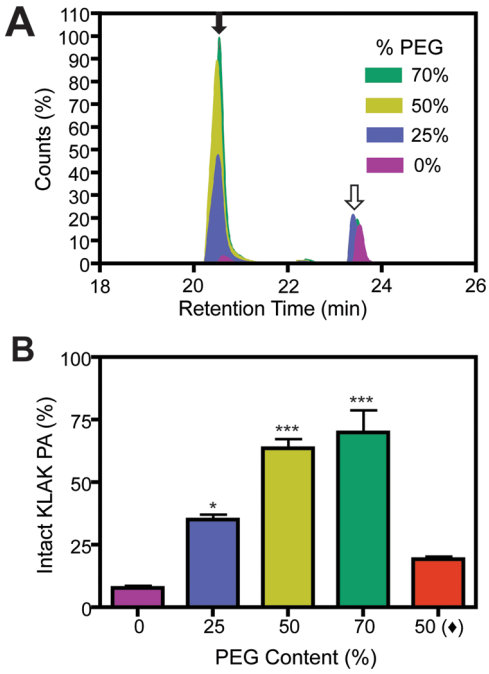

Figure 3. Enzymatic degradation. (A) The percentage of intact KLAK PA, as measured by LC/MS, increases with increasing concentrations of PEG PA. The solid arrow points to the KLAK PA peak, and the open arrow points to the internal standard, kept constant in all runs. (B) Quantification of intact KLAK PA. The addition of PEG PA prevents trypsin degradation. The 50(♦) bar represents a solution of KLAK and PEG PA that was preassembled separately prior to mixing and exposing to trypsin. (*$p < 0.001$, *$p < 0.05$).**

***In Vitro* Cytotoxicity.** We tested the cytotoxicity of KLAK PA on human breast cancer cells to determine if mixing with PEG PA affected the ability of KLAK PA to kill cells through membrane lysis.[24] *In vitro* results show that the mixture of the PEG PA and KLAK PA has no negative effect on cytotoxicity relative to the activity of KLAK PA alone (Figure 4A). Flow cytometry was used with DAPI staining to quantify membrane permeabilization of MCF7 breast cancer cells as a function of time (Figure 4B). Mitochondrial membranes also show loss of integrity (Figure 4C) with coassembled PA treatment. These results indicate that addition of 50 mol %

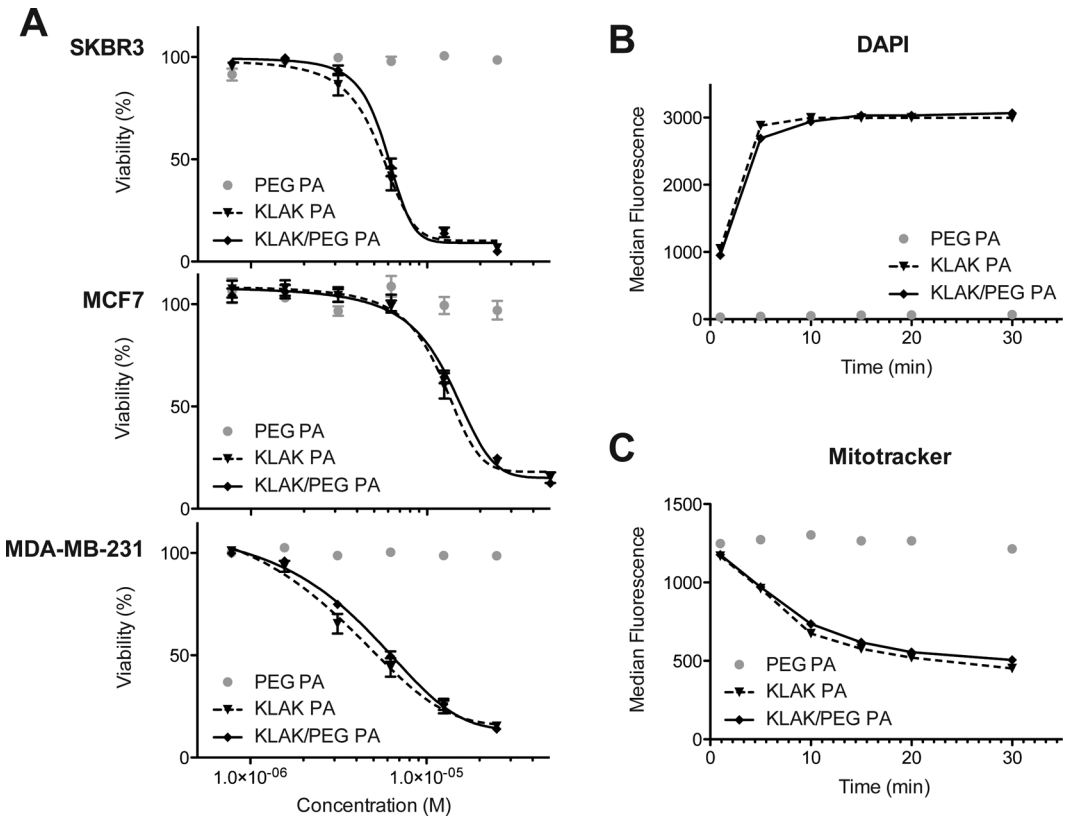

Figure 4. *In vitro* **cytotoxicity. (A) MDA-MB-231, MCF7, and SKBR3 human breast cancer cells were treated as indicated for 24 h, and viability was quantified using a MTS assay. MCF7 human breast cancer cells were treated as indicated, and intracellular DAPI (B) and Mitotracker red (C) fluorescence was determined by flow cytometry to assess the plasma and mitochondrial membrane integrity.**

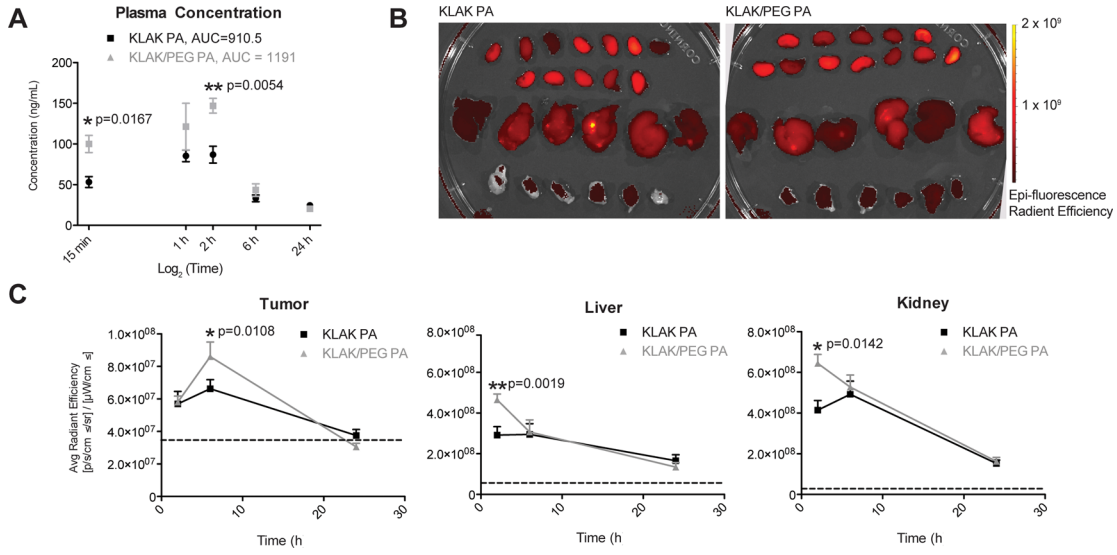

Figure 5. PA plasma and tissue biodistribution. (A) Quantification of plasma fluorescence, $n = 6$ per time point. (B) Tissue fluorescence following intraperitoneal administration of KLAK PA covalently modified with Alexa 700 to tumor-bearing mice; tissues from the 6 h time point are shown. (C) Quantification of fluorescence as average radiant efficiency ($n = 6$ animals per time point) comparing the signal in tissues from animals treated with KLAK PA alone or KLAK/PEG PA; the dashed line represents background fluorescence observed in control untreated animals. Statistical significance in all panels as measured by Student's *t* test is noted.

PEG PA does not produce any change in the rate of membrane lysis by KLAK PA. As expected, PEG PA alone showed no cytotoxicity up to a concentration of 1 mM. Thus, while mixing of PEG PA with KLAK PA does appear to limit enzyme access to the cationic peptides of KLAK PA, it does not appear to inhibit any interaction

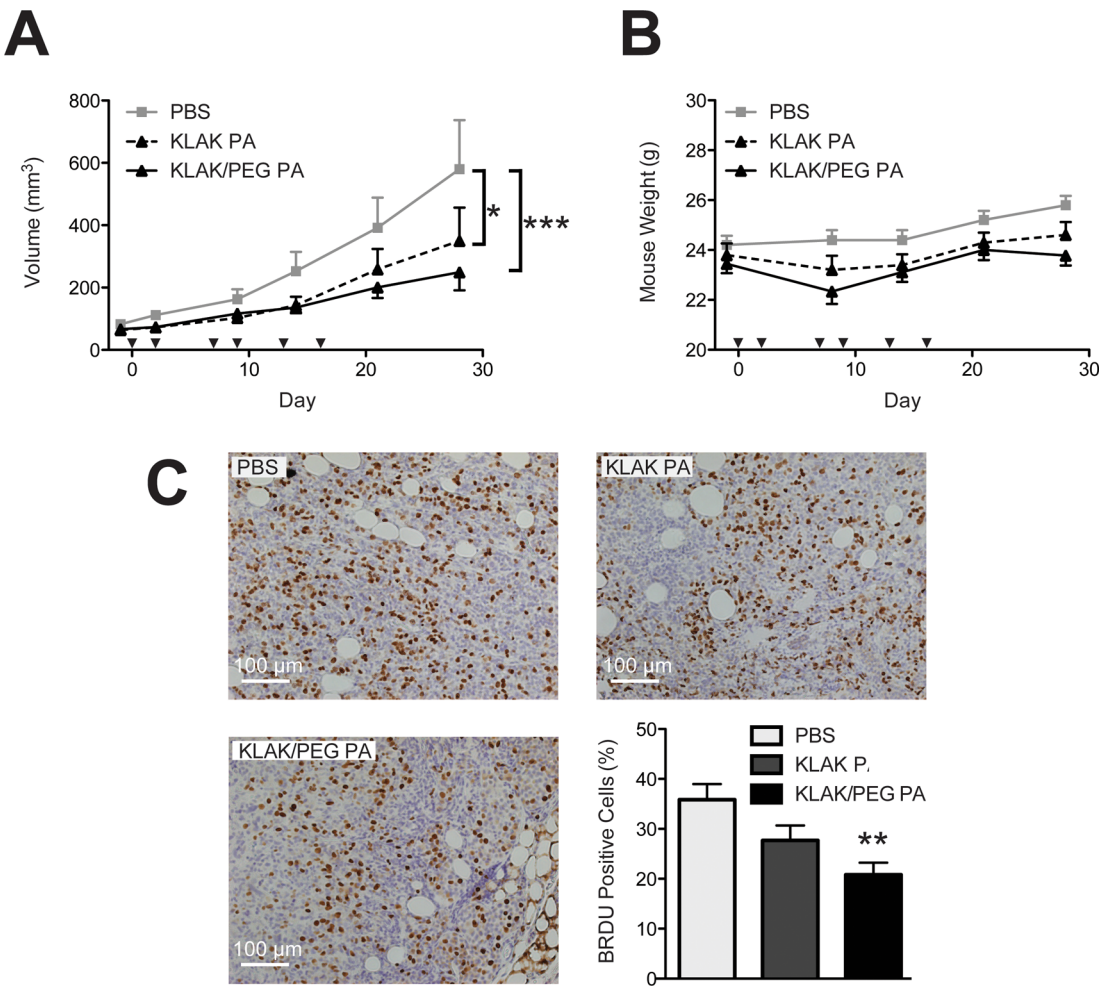

Figure 6. ***In vivo*** **antitumor activity. (A) The growth of MDA-MB-231 human breast cancer orthotopic tumors is inhibited by intraperitoneal treatment (inverted arrows) of KLAK PA nanostructures. Both the KLAK- and KLAK/PEG PA-treated tumors were statistically smaller, as determined by two-way ANOVA. (B) Mouse weights across groups were similar, suggesting the nanostructure treatment was well tolerated. (C) BRDU staining as a measure of cellular proliferation was statistically lower by one-way ANOVA in the L-KLAK PA-treated tumors when coassembled with PEG PA.**

of KLAK PA with cellular membranes. KLAK PA and D-KLAK PA showed no significant differences in cytotoxicity (Supplemental Figure S7).

PA Plasma and Tissue Biodistribution. We attempted to quantify the tissue-specific and plasma PA concentration over time by covalently attaching the near-IR dye Alexa 700 to the KLAK PA monomer. Following IP administration, blood from each mouse was collected at earlier time points by tail bleed, followed by intracardiac puncture as part of a terminal procedure, at which time tissues were harvested. The plasma fluorescence signal of KLAK-PEG PA-treated animals rose more rapidly relative to KLAK PA (Figure 5A), and more signal was seen in all tissues at 1 h (Figure 5B, C), suggesting it is more rapidly mobilized from the peritoneal compartment than KLAK PA alone. Fluorescence of both KLAK PA alone and KLAK-PEG PA mixtures was predominantly localized to liver and kidney (Figure 5B, C). Fluorescence observed in lung was minimal, speaking to the solubility of the PA fibers (data not shown). Area under the curve calculations indicated that plasma (Figure 5A) bioavailability is improved by the addition of PEG PA. Nevertheless, the observed plasma half-lives are on the order of several hours both with and without the addition of PEG PA, which is better than typical times observed for free peptides, suggesting the PA fibers are intrinsically resistant to degradation and/or elimination.[28,29] A limitation of using a fluorescence-based approach to quantify *in vivo* PA distribution is that the dye signal may be from a mixture of intact and degraded KLAK PA; in addition, the dye may alter the absorption, distribution, and elimination of the fibers. Because of the membrane lytic action of KLAK PA, off-target destruction of circulating blood cells was a theoretical concern. However, 24 h after PA administration no significant difference in white or red blood cell number was observed (Supplemental Table S1). Among the many metabolic parameters measured in the treated mice, alkaline phosphatase levels were significantly lower in the KLAK- and KLAK/PEG PA-treated animals compared with PBS-treated controls, and the KLAK PA-treated

animals had significantly higher blood glucose levels (Supplemental Table S2).

***In Vivo* Antitumor Activity.** An orthotopic mouse breast cancer model was used to measure the antitumor activity following intraperitoneal injection of KLAK PA. Treatment with both KLAK PA alone and KLAK/PEG PA significantly suppressed human MDA-MB-231 breast cancer growth in the mice relative to PBS alone (Figure 6A). There was a trend toward smaller tumors in the mice treated with the KLAK/PEG PA compared with those treated with the KLAK PA alone, but this difference was not statistically significant (Figure 6A). No significant change in average mouse weights were noted during treatment (Figure 6B), indicating that treatment was generally well-tolerated. Immunohistological staining for bromodeoxyuridine (BrdU) revealed a trend toward a reduction in the percentage of proliferating cells with all KLAK PA treatments that was statistically significant only when KLAK PA was given coassembled with PEG (Figure 6C). Our BrdU staining results corroborate a previous report demonstrating that nanoparticle delivery of membrane lytic peptides targets proliferating cancer cells.[25] Tumors of D-KLAK PA-treated mice trended smaller (Supplemental Figure S8), but unlike KLAK PA, only D-KLAK/PEG PA treatment resulted in statistically significant tumor inhibition (Supplemental Figure S8C). Because KLAK and D-KLAK PA performed similarly, we speculate that the clearance of KLAK PA is not determined by the stereochemistry of the molecule. This phenomenon has been observed when L-lysine and D-lysine were conjugated to monoclonal antibodies and injected systemically into mice; similar changes in renal clearance were observed.[43] An alternate possibility is that tumor targeting and antitumor action happen more rapidly than the PAs are cleared.

CONCLUSIONS

Self-assembled peptide amphiphiles offer a new and versatile platform as nanoscale cancer therapeutics. Here we have demonstrated that a membrane-lytic peptide amphiphile coassembles with a pegylated peptide amphiphile into cylindrical nanostructures to create filaments with greater proteolytic resistance than and similar *in vitro* anti-breast cancer cytotoxic activity to those based only on the lytic peptide. Furthermore, systemic delivery of these nanoscale filaments decreased breast cancer growth over four weeks of administration in a mouse xenograft model and appeared to be well-tolerated by the animals. This work highlights the potential of PA nanostructures as a biodegradable and customizable tumoricidal nanotechnology platform. We expect that the antitumor activity of PA nanostructures may be further enhanced through the use of chemotherapeutic drugs safely encapsulated in the nanofiber core. Furthermore, systemic toxicity may be reduced and tumor activity enhanced by the coassembly approach described here but using selective tumor-homing peptides.

MATERIALS AND METHODS

PA Synthesis and Materials Characterization. PAs were synthesized using standard Fmoc solid-phase synthesis conditions. Coupling reactions were performed using Fmoc-amino acids (4 equiv), HBTU (3.95 equiv), and diispropylethylamine (DIEA) (6 equiv) in dimethylformamide (DMF). Synthesis of L-KLAK PA and D-KLAK PA was achieved using L-amino acids and D-amino acids, respectively. For the hydrophobic tail of PEG PA (sequence $K(C_{12})A_4G_3E_3$-PEG), lauric acid was attached to the ε-amine of a lysine, which was deprotected by selective removal of the Mtt (Mtt = 4-methyltrityl) group using 4% trifluoroacetic acid (TFA) + 5% triisopropylsilane (TIPS) in CH_2Cl_2. CH_3O-PEG-COOH (MW 2000) was prepared as previously described[44] and attached on resin at the N-terminus of the PEG PA. The alkyl tail of the KLAK PA was formed by reacting the N-terminus with palmitic acid (4 equiv), HBTU (3.95 equiv), and DIEA (6 equiv) in DMF. Following cleavage using a TFA/TIPS/H_2O mixture (95:2.5:2.5), PAs were purified by high-performance liquid chromatography (HPLC).

Purification by preparative-scale HPLC was carried out on a Varian Prostar 210 HPLC system, eluting with 2% acetonitrile (ACN) to 100% ACN in water on a Phenomenex C18 Gemini NX column (150 × 30 mm) with 5 μm pore size and 110 Å particle size. A 0.1% NH_4OH or 0.1% trifluoroacetic acid solution, for acidic or basic PAs, respectively, was added to both mobile phases to aid PA solubility. Product-containing fractions were confirmed by ESI mass spectrometry (Agilent 6510 Q-TOF LC/MS), combined, and lyophilized after removing ACN by rotary evaporation. Amino acid analyses were performed by Commonwealth Biotechnologies (Richmond, VA, USA).

Coassembly of the PAs was achieved by dissolving the KLAK PA and PEG PA separately in hexafluoroisopropanol, an organic solvent known to disrupt hydrogen bonds,[45−47] and then mixed together for at least 15 min. Samples were lyophilized to dryness to form a powder, as previously reported by our group.[48] After lyophilization in HFIP, samples were dissolved in water, aliquoted, and lyophilized again.

A KLAK PA-AlexaFluor 700 conjugate was synthesized by reacting a 5 molar excess of KLAK PA with NHS-AlexaFluor 700 (Invitrogen). KLAK PA was dissolved in DMSO at a concentration of 0.5 mM with 1% triethylamine, and AlexaFluor 700 was added dropwise to a stirring solution and reacted overnight (the reaction was confirmed using ESI mass spectrometry). The KLAK PA-AlexaFluor 700 conjugate was dialyzed in H_2O overnight to remove any unreacted dye and subsequently lyophilized. KLAK PA-AlexaFluor 700 and PEG PA mixtures were coassembled in HFIP, as described above.

Specimens for conventional transmission electron microscopy were prepared by drop-casting samples on carbon type B copper grids (Ted Pella) followed by staining with a 2% uranyl acetate aqueous solution. Cryogenic TEM (cryo-TEM) specimens were prepared using an FEI Vitrobot by blotting in 95% humidity and subsequently plunging grids into liquid ethane. Images were taken for both conventional and cryo-TEM using a JEOL 1230 transmission electron microscope operating at 100 keV equipped with a Gatan camera.

Small-angle X-ray scattering experiments were performed at the Advanced Photon Source, Argonne National Laboratory. The X-ray energy (15 keV) was selected using a double-crystal monochromator, and the SAXS CCD camera was offset in order to achieve a wide range of scattering angles. Samples were dissolved at a concentration of 2 mM and placed in 1.5 mm quartz capillary tubes. The typical incident X-ray flux on the sample was $\sim 1 \times 10^{12}$ photons/s with a 0.2 × 0.3 mm^2

collimator, estimated by a He ion channel, and samples were irradiated for 5 s. The 1D scattering profiles were obtained by radial integration of the 2D patterns, with scattering from the capillaries subtracted as background. Scattering profiles were then plotted on a relative scale as a function of the scattering vector $q = (4\pi/\lambda)\sin(\theta/2)$, where θ is the scattering angle.

1H-Diffusion ordered spectroscopy was performed using a Bruker Avance 600 MHz spectrometer at ambient temperature. For these experiments samples were dissolved at a constant total concentration of PA (5 mM KLAK PA alone or 2.5 mM KLAK PA and 2.5 mM PEG PA in the mixed case) in 99.9% D_2O (Sigma), and 32 points were measured with a 7 μs 90-degree pulse. Diffusion data were processed and analyzed using DOSY Toolbox.[49]

***In Vitro* Enzyme Degradation Kinetics.** Enzyme degradation was performed using trypsin, which was conjugated to agarose beads (Sigma). KLAK PA alone or KLAK PA with PEG PA ($n = 3$ for each group) was mixed in PBS for 1 h with 2 units of trypsin under constant agitation at room temperature. The samples were subsequently centrifuged at 500 g for 30 s, and the supernatant was removed from the trypsin beads. Samples were diluted 10-fold into a solution with an internal standard, $C_{16}V_3A_3K_3$-$(OEG)_5$-NH_2, with a concentration that was held constant for all injections. LC/MS was performed, and the total ion counts were quantified for intact KLAK PA and compared to undigested KLAK PA controls.

***In Vitro* Breast Cancer Cytotoxicity.** The *in vitro* growth of cell cultures was measured using the CellTiter 96 Aqueous One Solution cell proliferation assay (Promega, Madison WI, USA). The cell titer assay is a 3-(4,5-dimethylthiazol-2-yl)-5-(3-carboxymethoxyphenyl)-2-(4-sulfophenyl)-2*H*-tetrazolium (MTS)-based assay and was used according to the supplier's instructions. For each well to be assayed in a 96-well plate containing 100 μL of media per well, 20 μL of the CellTiter96 Aqueous One Solution was added. The plate was incubated for 1−3 h at 37 °C, and absorbance was read using a Molecular Devices microplate reader (490 nm).

Membrane Permeability Assays. Cells were labeled with 50 nM Mitotracker Red (Invitrogen) to stain mitochondrial membranes according to the manufacturer's instructions. After trypsinization, cells (1×10^6 cells/mL) were resuspended in PBS and 100 ng/mL DAPI was added. Fluorescence intensity at 25 °C was measured using a DakoCyomation CyAn.

***In Vivo* Orthotopic Breast Cancer Model.** MDA-MB-231 human breast ductal carcinoma cells (1×10^6) were injected intraductally into the fourth mammary fat pads of 4−5-week-old female athymic nude mice (Harlan Sprague−Dawley, Madison, WI, USA) to establish orthotopic xenograft tumors. Four weeks after tumor implantation, mice were randomized into treatment groups (8 mice per group) and administered either PBS vehicle (Sigma-Aldrich), KLAK PA 14 mg/kg/dose, or KLAK PA 14 mg/kg/dose encapsulated with 1 molar equiv of PEG PA by intraperitoneal (ip) injection twice per week for six total injections. Intraperitoneal administration of nanoparticles has been shown to cause a delay in the rise of circulating nanoparticle concentration relative to intravenous (iv) administration; however in preliminary experiments we found similar levels of fluorescent PA signal in mouse mammary tumor xenografts following either ip or iv administration (data not shown), which given the lower success rate of mouse tail vein injections led us to choose ip treatments for our experiments.[50] Tumors were measured after each injection with Vernier calipers, and tumor volume was calculated using the following, previously described,[51] equation: tumor volume (mm^3) = (length × width^2) × $\pi/6$. All animal experiments were conducted under protocols approved by the Animal Care and Use Committee of Northwestern University.

PA Plasma Kinetics and Tissue Biodistribution. We determined the fate of KLAK PA-AlexaFluor 700 either alone or coassembled with PEG PA in athymic nude mice unilaterally bearing MDA-MB-231 tumors as described above. KLAK PA was injected at a concentration of 20 mg/kg (1.8 mM) with 2.5 μg of conjugated AlexaFluor 700 dye. For the KLAK PA with PEG PA, the concentrations of KLAK and dye were kept constant, and 27 mg/kg (1.8 mM) of PEG PA was added. Blood was collected either as a terminal procedure *via* cardiac puncture or by tail vein bleeds into heparinized capillary tubes. Following centrifugation at 10 000 rpm for 10 min, a Molecular Devices SpectraMax M5 plate reader was used for quantification of plasma fluorescence. Mice were euthanized at the specified time points, and tissues were harvested and stored in 4% paraformaldehyde for subsequent fluorescence quantification using a Caliper Life Sciences IVIS Spectrum Bioluminescence System. Blood collected from animals 24 h following PA or PBS administration was sent to RADIL for metabolic profiling and complete blood count.

Statistical Analysis. Statistical significance was assessed using Graph-Pad Prism 5.0b software using the appropriate statistical test: two-way ANOVA with Bonferroni post-tests for *in vivo* tumor cytotoxicity and peripheral smear/metabolic profiling studies, one-way ANOVA with Dunnett post-tests for tissue fluorescence studies, or one-way ANOVA with Bonferroni post-test for the enzyme degradation studies.

Conflict of Interest: The authors declare no competing financial interest.

Acknowledgment. This work was supported by NCI Center for Cancer Nanotechnology Excellence grant 1U54CA119341 (S.I.S. and V.L.C.); the Breast Cancer Research Foundation (V.L.C.); Dixon Translational Research grant (V.L.C. and S.I.S.); Department of Defense Breast Cancer Research Program grant W81XWH-10-1-0503 (D.J.T.); NIH grants 5F32GM080021 (S.M.S.) and T32DK007169 (D.J.T.); and a Graduate Research Fellowship from the National Science Foundation (T.J.M.). Additional support was provided by the Northwestern University Flow Cytometry Facility and a Robert H. Lurie Comprehensive Cancer Center Support grant (NCI CA060553). Imaging work was performed at the Northwestern University Cell Imaging Facility generously supported by NCI CCSG P30 CA060553 awarded to the Robert H. Lurie Comprehensive Cancer Center. NMR experiments were performed at the Integrated Molecular Structure Education and Research Center at Northwestern University. TEM images were taken in the Biological Imaging Facility at Northwestern University. SAXS experiments were performed at the DuPont-Northwestern-Dow Collaborative Access Team (DND-CAT) located at Sector 5 of the Advanced Photon Source (APS). DND-CAT is supported by E.I. DuPont de Nemours & Co., The Dow Chemical Company, and Northwestern University. Use of the APS, an Office of Science User Facility operated for the U.S. Department of Energy (DOE) Office of Science by Argonne National Laboratory, was supported by the U.S. DOE under Contract No. DE-AC02-06CH11357. The authors are grateful to Steven Weigand for assistance with SAXS experiments. We thank Dr. Honggang Cui, Dr. Stephen Soukasene, Dr. John Matson, and Dr. Liam Palmer for helpful discussions.

Supporting Information Available: This material is available free of charge via the Internet at http://pubs.acs.org.

REFERENCES AND NOTES

1. Petros, R. A.; DeSimone, J. M. Strategies in the Design of Nanoparticles for Therapeutic Applications. *Nat. Rev. Drug Discovery* **2010**, *9*, 615–627.
2. Peer, D.; Karp, J. M.; Hong, S.; Farokhzad, O. C.; Margalit, R.; Langer, R. Nanocarriers as an Emerging Platform for Cancer Therapy. *Nat. Nanotechnol.* **2007**, *2*, 751–760.
3. Matsumura, Y.; Maeda, H. A New Concept for Macromolecular Therapeutics in Cancer Chemotherapy: Mechanism of Tumoritropic Accumulation of Proteins and the Antitumor Agent Smancs. *Cancer Res.* **1986**, *46*, 6387–6392.
4. Steinmetz, N. F.; Mertens, M. E.; Taurog, R. E.; Johnson, J. E.; Commandeur, U.; Fischer, R.; Manchester, M. Potato Virus X As a Novel Platform for Potential Biomedical Applications. *Nano Lett.* **2010**, *10*, 305–312.
5. Geng, Y.; Dalhaimer, P.; Cai, S.; Tsai, R.; Tewari, M.; Minko, T.; Discher, D. E. Shape Effects of Filaments *Versus* Spherical Particles in Flow and Drug Delivery. *Nat. Nanotechnol.* **2007**, *2*, 249–255.
6. Christian, D. A.; Cai, S.; Garbuzenko, O. B.; Harada, T.; Zajac, A. L.; Minko, T.; Discher, D. E. Flexible Filaments for *in Vivo*

Imaging and Delivery: Persistent Circulation of Filomicelles Opens the Dosage Window for Sustained Tumor Shrinkage. *Mol. Pharmaceutics* **2009**, *6*, 1343–1352.
7. Zhang, K.; Rossin, R.; Hagooly, A.; Chen, Z.; Welch, M. J.; Wooley, K. L. Folate-Mediated Cell Uptake of Shell-Cross-linked Spheres and Cylinders. *J. Polym. Sci. Part A-1: Polym. Chem.* **2008**, *46*, 7578–7583.
8. Hartgerink, J. D.; Beniash, E.; Stupp, S. I. Self-Assembly and Mineralization of Peptide-Amphiphile Nanofibers. *Science* **2001**, *294*, 1684–1688.
9. Hartgerink, J. D.; Beniash, E.; Stupp, S. I. Peptide-Amphiphile Nanofibers: A Versatile Scaffold for the Preparation of Self-Assembling Materials. *Proc. Natl. Acad. Sci. U. S. A.* **2002**, *99*, 5133–5138.
10. Silva, G. A.; Czeisler, C.; Niece, K. L.; Beniash, E.; Harrington, D. A.; Kessler, J. A.; Stupp, S. I. Selective Differentiation of Neural Progenitor Cells by High-Epitope Density Nanofibers. *Science* **2004**, *303*, 1352–1355.
11. Tysseling-Mattiace, V. M.; Sahni, V.; Niece, K. L.; Birch, D.; Czeisler, C.; Fehlings, M. G.; Stupp, S. I.; Kessler, J. A. Self-Assembling Nanofibers Inhibit Glial Scar Formation and Promote Axon Elongation after Spinal Cord Injury. *J. Neurosci.* **2008**, *28*, 3814–3823.
12. Shah, R. N.; Shah, N. A.; Del Rosario Lim, M. M.; Hsieh, C.; Nuber, G.; Stupp, S. I. Regenerative Medicine Special Feature: Supramolecular Design of Self-Assembling Nanofibers for Cartilage Regeneration. *Proc. Natl. Acad. Sci. U. S. A.* **2010**, *107*, 3293–3298.
13. Mata, A.; Geng, Y.; Henrikson, K. J.; Aparicio, C.; Stock, S. R.; Satcher, R. L.; Stupp, S. I. Bone Regeneration Mediated by Biomimetic Mineralization of a Nanofiber Matrix. *Biomaterials* **2010**, *31*, 6004–6012.
14. Webber, M. J.; Tongers, J.; Renault, M.-A.; Roncalli, J. G.; Losordo, D. W.; Stupp, S. I. Development of Bioactive Peptide Amphiphiles for Therapeutic Cell Delivery. *Acta Biomater.* **2010**, *6*, 3–11.
15. Webber, M. J.; Han, X.; Murthy, S. N. P.; Rajangam, K.; Stupp, S. I.; Lomasney, J. W. Capturing the Stem Cell Paracrine Effect Using Heparin-Presenting Nanofibres to Treat Cardiovascular Diseases. *J. Tissue Eng. Regener. Med.* **2010**, *4*, 600–610.
16. Webber, M. J.; Tongers, J.; Newcomb, C. J.; Marquardt, K.-T.; Bauersachs, J.; Losordo, D. W.; Stupp, S. I. Supramolecular Nanostructures that Mimic VEGF as a Strategy for Ischemic Tissue Repair. *Proc. Natl. Acad. Sci. U. S. A.* **2011**, *108*, 13438–13443.
17. Soukasene, S.; Toft, D. J.; Moyer, T. J.; Lu, H.; Lee, H.-K.; Standley, S. M.; Cryns, V. L.; Stupp, S. I. Antitumor Activity of Peptide Amphiphile Nanofiber-Encapsulated Camptothecin. *ACS Nano* **2011**, *5*, 9113–9121.
18. Hupp, T. R.; Sparks, A.; Lane, D. P. Small Peptides Activate the Latent Sequence-Specific DNA Binding Function of p53. *Cell* **1995**, *83*, 237–245.
19. Murphy, E. A.; Majeti, B. K.; Barnes, L. A.; Makale, M.; Weis, S. M.; Lutu-Fuga, K.; Wrasidlo, W.; Cheresh, D. A. Nanoparticle-Mediated Drug Delivery to Tumor Vasculature Suppresses Metastasis. *Proc. Natl. Acad. Sci. U. S. A.* **2008**, *105*, 9343–9348.
20. Javadpour, M. M.; Juban, M. M.; Lo, W. C.; Bishop, S. M.; Alberty, J. B.; Cowell, S. M.; Becker, C. L.; McLaughlin, M. L. *De Novo* Antimicrobial Peptides with Low Mammalian Cell Toxicity. *J. Med. Chem.* **1996**, *39*, 3107–3113.
21. Ellerby, H. M.; Arap, W.; Ellerby, L. M.; Kain, R.; Andrusiak, R.; Rio, G. D.; Krajewski, S.; Lombardo, C. R.; Rao, R.; Ruoslahti, E.; *et al*. Anti-Cancer Activity of Targeted Pro-Apoptotic Peptides. *Nat. Med. (N. Y., NY, U. S.)* **1999**, *5*, 1032–1038.
22. Papo, N.; Seger, D.; Makovitzki, A.; Kalchenko, V.; Eshhar, Z.; Degani, H.; Shai, Y. Inhibition of Tumor Growth and Elimination of Multiple Metastases in Human Prostate and Breast Xenografts by Systemic Inoculation of a Host Defense-Like Lytic Peptide. *Cancer Res.* **2006**, *66*, 5371–5378.
23. Mai, J. C.; Mi, Z.; Kim, S. H.; Ng, B.; Robbins, P. D. A Proapoptotic Peptide for the Treatment of Solid Tumors. *Cancer Res.* **2001**, *61*, 7709–7712.
24. Standley, S. M.; Toft, D. J.; Cheng, H.; Soukasene, S.; Chen, J.; Raja, S. M.; Band, V.; Band, H.; Cryns, V. L.; Stupp, S. I. Induction of Cancer Cell Death by Self-Assembling Nanostructures Incorporating a Cytotoxic Peptide. *Cancer Res.* **2010**, *70*, 3020–3026.
25. Soman, N. R.; Baldwin, S. L.; Hu, G.; Marsh, J. N.; Lanza, G. M.; Heuser, J. E.; Arbeit, J. M.; Wickline, S. A.; Schlesinger, P. H. Molecularly Targeted Nanocarriers Deliver the Cytolytic Peptide Melittin Specifically to Tumor Cells in Mice, Reducing Tumor Growth. *J. Clin. Invest.* **2009**, *119*, 2830–2842.
26. Papo, N.; Shai, Y. New Lytic Peptides Based on the D,L-Amphipathic Helix Motif Preferentially Kill Tumor Cells Compared to Normal Cells. *Biochemistry* **2003**, *42*, 9346–9354.
27. Sugahara, K. N.; Teesalu, T.; Karmali, P. P.; Kotamraju, V. R.; Agemy, L.; Girard, O. M.; Hanahan, D.; Mattrey, R. F.; Ruoslahti, E. Tissue-Penetrating Delivery of Compounds and Nanoparticles into Tumors. *Cancer Cell* **2009**, *16*, 510–520.
28. McGregor, D. P. Discovering and Improving Novel Peptide Therapeutics. *Curr. Opin. Pharmacol.* **2008**, *8*, 616–619.
29. Werle, M.; Bernkop-Schnurch, A. Strategies to Improve Plasma Half Life Time of Peptide and Protein Drugs. *Amino Acids* **2006**, *30*, 351–367.
30. Papo, N.; Braunstein, A.; Eshhar, Z.; Shai, Y. Suppression of Human Prostate Tumor Growth in Mice by a Cytolytic D-, L-Amino Acid Peptide: Membrane Lysis, Increased Necrosis, and Inhibition of Prostate-Specific Antigen Secretion. *Cancer Res.* **2004**, *64*, 5779–5786.
31. Joralemon, M. J.; McRae, S.; Emrick, T. PEGylated Polymers for Medicine: From Conjugation to Self-Assembled Systems. *Chem. Commun. (Cambridge, U. K.)* **2010**, *46*, 1377–1393.
32. Grunwald, J.; Rejtar, T.; Sawant, R.; Wang, Z.; Torchilin, V. P. TAT Peptide and its Conjugates: Proteolytic Stability. *Bioconjugate Chem.* **2009**, *20*, 1531–1537.
33. Gabizon, A.; Shmeeda, H.; Barenholz, Y. Pharmacokinetics of PEGylated Liposomal Doxorubicin: Review of Animal and Human Studies. *Clin. Pharmacokinet.* **2003**, *42*, 419–436.
34. Photos, P. J.; Bacakova, L.; Discher, B.; Bates, F. S.; Discher, D. E. Polymer Vesicles *in Vivo*: Correlations with PEG Molecular Weight. *J. Controlled Release* **2003**, *90*, 323–334.
35. Mosqueira, V. C.; Legrand, P.; Morgat, J. L.; Vert, M.; Mysiakine, E.; Gref, R.; Devissaguet, J. P.; Barratt, G. Biodistribution of Long-Circulating PEG-Grafted Nanocapsules in Mice: Effects of PEG Chain Length and Density. *Pharm. Res.* **2001**, *18*, 1411–1419.
36. Duncan, R. The Dawning Era of Polymer Therapeutics. *Nat. Rev. Drug Discovery* **2003**, *2*, 347–360.
37. Collier, J.; Messersmith, P. Self-Assembling Polymer-Peptide Conjugates: Nanostructural Tailoring. *Adv. Mater. (Weinheim, Ger.)* **2004**, *16*, 907–910.
38. Burkoth, T.; Benzinger, T.; Urban, V.; Lynn, D.; Meredith, S.; Thiyagarajan, P. Self-Assembly of a Beta((10−35))-PEG Block Copolymer Fibrils. *J. Am. Chem. Soc.* **1999**, *121*, 7429–7430.
39. Hamley, I. W.; Ansari, I. A.; Castelletto, V.; Nuhn, H.; Rosler, A.; Klok, H. A. Solution Self-Assembly of Hybrid Block Copolymers Containing Poly(Ethylene Glycol) and Amphiphilic Beta-Strand Peptide Sequences. *Biomacromolecules* **2005**, *6*, 1310–1315.
40. Niece, K.; Hartgerink, J.; Donners, J.; Stupp, S. Self-Assembly Combining Two Bioactive Peptide-Amphiphile Molecules into Nanofibers by Electrostatic Attraction. *J. Am. Chem. Soc.* **2003**, *125*, 7146–7147.
41. Cohen, Y.; Avram, L.; Frish, L. Diffusion NMR Spectroscopy in Supramolecular and Combinatorial Chemistry: An Old Parameter--New Insights. *Angew. Chem., Int. Ed.* **2005**, *44*, 520–554.
42. Marega, R.; Aroulmoji, V.; Bergamin, M.; Feruglio, L.; Dinon, F.; Bianco, A.; Murano, E.; Prato, M. Two-Dimensional Diffusion-Ordered NMR Spectroscopy as a Tool for Monitoring Functionalized Carbon Nanotube Purification and Composition. *ACS Nano* **2010**, *4*, 2051–2058.

43. Behr, T. M.; Sharkey, R. M.; Juweid, M. E.; Blumenthal, R. D.; Dunn, R. M.; Griffiths, G. L.; Bair, H. J.; Wolf, F. G.; Becker, W. S.; Goldenberg, D. M. Reduction of the Renal Uptake of Radiolabeled Monoclonal Antibody Fragments by Cationic Amino Acids and their Derivatives. *Cancer Res.* **1995**, *55*, 3825–3834.
44. Masson, C.; Scherman, D.; Bessodes, M. 2,2,6,6-Tetramethyl-1-Piperidinyl-Oxyl/[Bis(Acetoxy)-Iodo]Benzene-Mediated Oxidation: A Versatile and Convenient Route to Poly(Ethylene Glycol) Aldehyde or Carboxylic Acid Derivatives. *J. Polym. Sci., Part A: Polym. Chem.* **2001**, *39*, 4022–4024.
45. Sirangelo, I.; Dal Piaz, F.; Malmo, C.; Casillo, M.; Birolo, L.; Pucci, P.; Marino, G.; Irace, G. Hexafluoroisopropanol and Acid Destabilized Forms of Apomyoglobin Exhibit Structural Differences. *Biochemistry* **2003**, *42*, 312–319.
46. Ha, S. W.; Asakura, T.; Kishore, R. Distinctive Influence of Two Hexafluoro Solvents on the Structural Stabilization of Bombyx Mori Silk Fibroin Protein and its Derived Peptides: ^{13}C NMR and CD Studies. *Biomacromolecules* **2006**, *7*, 18–23.
47. Crisma, M.; Saviano, M.; Moretto, A.; Broxterman, Q. B.; Kaptein, B.; Toniolo, C. Peptide Alpha/3(10)-Helix Dimorphism in the Crystal State. *J. Am. Chem. Soc.* **2007**, *129*, 15471–15473.
48. Matson, J. B.; Stupp, S. I. Drug Release from Hydrazone-Containing Peptide Amphiphiles. *Chem. Commun. (Cambridge, U. K.)* **2011**, *47*, 7962–7964.
49. Nilsson, M. The DOSY Toolbox: A New Tool for Processing PFG NMR Diffusion Data. *J. Magn. Reson.* **2009**, *200*, 296–302.
50. Lin, Y.-Y.; Li, J.-J.; Chang, C.-H.; Lu, Y.-C.; Hwang, J.-J.; Tseng, Y.-L.; Lin, W.-J.; Ting, G.; Wang, H.-E. Evaluation of Pharmacokinetics of In-111-Labeled VNB-Pegylated Liposomes after Intraperitoneal and Intravenous Administration in a Tumor/Ascites Mouse Model. *Cancer Biother. Radiopharm.* **2009**, *24*, 453–460.
51. Lu, M.; Kwan, T.; Yu, C.; Chen, F.; Freedman, B.; Schafer, J. M.; Lee, E. J.; Jameson, J. L.; Jordan, V. C.; Cryns, V. L. Peroxisome Proliferator-Activated Receptor Gamma Agonists Promote TRAIL-Induced Apoptosis by Reducing Survivin Levels *via* Cyclin D3 Repression and Cell Cycle Arrest. *J. Biol. Chem.* **2005**, *280*, 6742–6751.